RESEARCH PAPER

Effects of wall perturbations on the stabilized FEM solution of steady MHD flow in a duct

Münevver Tezer-Sezgin [ID] [1,‡] and **Selçuk Han Aydın** [ID] [2,*,‡]

[1]Department of Mathematics, Middle East Technical University, Çankaya, 06800 Ankara, Türkiye,
[2]Department of Mathematics, Karadeniz Technical University, 61080 Trabzon, Türkiye

*Corresponding Author
‡munt@metu.edu.tr (Münevver Tezer-Sezgin); shaydin@ktu.edu.tr (Selçuk Han Aydın)

Abstract

In this study, the effects of curved boundary perturbations on the solution of steady magnetohydrodynamic (MHD) duct flow are investigated. Hartmann (upper and bottom) walls are perturbly curved and perfectly conducting while the side walls are insulated and plane. The velocity of the flow and induced magnetic field are obtained numerically by solving the steady MHD flow coupled equations using the finite element method (FEM with Streamline Upwind Petrov Galerkin (SUPG)) stabilization to inhibit instabilities in the flow. The results are obtained for Hartmann number (Ha) values up to 500, for several definitions of the curved upper and bottom walls, and for several values of perturbation parameters of the curved walls ($0 \leq \epsilon_u, \epsilon_b \leq 0.3$). The velocity and the induced magnetic field sensitivity to the curved wall shapes are visualized in terms of equivelocity and current lines. It is found that the flow and the induced magnetic field are affected by the curved boundary shapes especially near those boundaries and also, to some extent, in the whole duct. It is also observed that increasing the Hartman number pushes the flow near the upper boundary even if both upper and bottom walls are perturbed since the external magnetic field applies vertically. The increase in the perturbation parameter of the curved upper boundary forces the flow to move through this wall and the induced magnetic field reaches its maximum value near the maximum points of the perturbed curve. Further, an increase in Ha delays the effect of the curved boundaries and gives rise to flattened flow with side layers and stagnant fluid at the central part of the duct overwhelming the effects of curved boundaries.

Keywords: Steady MHD duct flow; stabilized FEM; perturbed boundary

AMS 2020 Classification: 76M10; 65N30; 80M10

1 Introduction

Magnetohydrodynamic (MHD) deals with the study of the motion of electrically conducting fluids in the presence of magnetic fields. The fluid motion is influenced by the magnetic field,

and this influence is expressed mathematically by including the electromagnetic force in the equations of motion. The electromagnetic force causes an electric current density to flow in the fluid. Then, the fluid motion changes in turn the magnetic field through Ohm's law determining the appearance within the fluid of an induced magnetic field. Thus, the Navier-Stokes equations from hydrodynamics and Maxwell's equations from electromagnetic phenomena must be solved simultaneously in terms of the velocity of the fluid and the induced magnetic field. The steady MHD duct flow problem for the incompressible, viscous, electrically conducting Newtonian fluids in channels and ducts under a uniform magnetic field has been first investigated by Hartmann [1]. The MHD duct flow has many physical, engineering, and biomedical applications such as designing cooling systems, nuclear reactors, MHD generators, pumps, accelerators, flow meters and blood flow measurement devices. The magnetic field is imposed either parallel or perpendicular to one pair of sides of the rectangular duct. Therefore, many researchers investigated the MHD duct flow problem either analytically or numerically. The exact solution to the problem can be obtained solely for some specific domain regions and/or boundary conditions which is given in [2]. Hence, most of the solutions to the MHD flow problems have been numerically obtained by using different methods. Some of these studies are achieved using the finite difference method (FDM) [3–5], the finite element method (FEM) [6–8], the boundary element method (BEM) [9, 10], the dual reciprocity boundary element method (DRBEM) [11] and the differential quadrature method (DQM) [12] for several geometrical cross-sections and different boundary conditions. MHD duct flow problems are solved using BEM (with the fundamental solution of coupled MHD equations) and DRBEM for different geometry, boundary conditions, and orientation of applied magnetic field in [13]. The finite element method is well suited to irregular domains and preferred for the curved boundaries as is the case in this study. The FDM, BEM, and DRBEM with linear elements are usually suitable for rectangular regions in 2-D. It is well known that [8, 14], in the standard Galerkin formulation of the MHD duct flow problem, there exist numerical instabilities for large Hartmann number (Ha) values. In order to eliminate these numerical instabilities either a sufficiently fine mesh should be used, which increases the computational cost, or a stabilization procedure should be implemented. For instance, the MHD duct flow problem was solved with a stabilized FEM using the residual-free bubble (RFB) functions for the high values of Hartmann number by Neslituark and Tezer-Sezgin [14, 15]. In some cases, the problem domain boundary exhibits some irregularities. In these cases, it is not possible to obtain the analytical solution to the problem. For instance, the numerical solution of the MHD duct flow problem with small perturbation on the upper boundary is obtained in [16] using an asymptotic analysis with respect to the perturbation parameters ϵ. Similarly, Aydin and Tezer-Sezgin [17] have investigated the same problem for a slipping upper perturbed boundary by using an asymptotic analysis for the perturbation and solving the MHD direct and Cauchy duct problems by the DRBEM only in the two-dimensional rectangular domain. The unsteady magnetohydrodynamic (MHD) flow with an upper perturbed boundary is also investigated in [18] by using DRBEM in space and a backward finite difference scheme for the time. It is shown that, with an increase in perturbation parameter the magnitude of the induced magnetic field increases. An additional vortex of the flow is formed at the center of the cavity and this vortex moves upwards through the expanded domain due to the perturbed upper boundary. Yang et al. [19] have solved the MHD duct flow problem for rectangular, and rectangular ducts with triangular strips on the walls. The effects of the strips have been given on the velocity distribution and the MHD pressure drop. The analytical solution of magnetohydrodynamic flow through a wavy curved channel having sinusoidal and periodic boundaries is considered by Okechi et al. [20] using the boundary perturbation method in order to obtain the velocity field and volumetric flow rate values. In Marusic-Paloka et al. [21], MHD flow through a channel filled with a porous medium with a slightly perturbed boundary is investigated.

They employ asymptotic analysis with respect to perturbation parameters together with error analysis. They have found that the effects of small boundary perturbations with respect to the *Ha* are non-local. A radial basis function-based FDM in Jeyanthi and Ganesh [22] has been used to adjust the width and magnitude of the perturbation on the wall for solving MHD flow in a duct.

In this study, the steady MHD flow in a long channel with a rectangular cross-section having both upper and lower perturbed boundaries is considered. It is the extension of the work presented in the conferences [23, 24] in which the perturbation is considered only for the upper boundary in [23]. The popular and widely-employed stabilized finite element method known as the Streamline Upwind Petrov-Galerkin (FEM with SUPG) method [25] is used as the solution procedure. The solutions are obtained for the Hartmann number values Ha $\leq$ 500 and for perturbation parameters $\{\epsilon_u, \epsilon_b\} \in \{0.0, 0.1, 0.2, 0.3\}$. Moreover, the perturbed boundaries are defined using different functions which are $\cos(\frac{2\pi}{3}x)$, $\cos(\frac{\pi}{4}x)$, $(4 - x^2)\cos(\pi x)$, $(4 - x^2)\sin(\pi x)$. Thus, the FEM with SUPG stabilization numerical procedure is able to capture the solution even in the irregularities of the wall for large *Ha* values in the MHD duct flow with considerably small system size.

2   Physical problem and mathematical modeling

As illustrated in Figure 1, the flow of an incompressible, viscous and electrically conducting Newtonian fluid is considered in a long channel of cross-section with plane-insulated vertical side walls and perfectly conducting bottom and top curved walls. There is a uniform steady pressure gradient $\frac{\partial p}{\partial z}$ in the channel-axis direction and a uniform steady external magnetic field with intensity B_0 applies in the $y-$direction. The flow is steady and fully-developed in the pipe-axis direction and the fluid is actually driven down by a steady and uniform pressure gradient and applied external magnetic field. Thus, the flow is two-dimensional in the duct having only axial normalized velocity component $V\mathbf{e}_z$ and induced normalized magnetic field component $B\mathbf{e}_z$ with $\mathbf{e}_z$ the unit vector in the z direction giving $V\mathbf{e}_z = V(x, y)$ and $B\mathbf{e}_z = B(x, y)$ in the duct. Moreover,
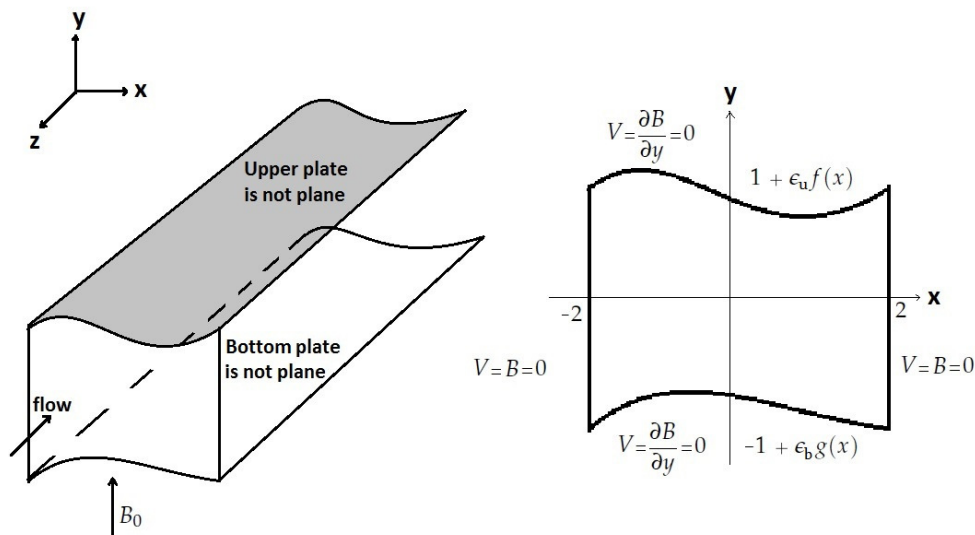

Figure 1. Liquid domain (left) and boundary conditions on the contour $\partial\Omega$ of the normalized cross-section Ω (right)

the upper and bottom boundaries of the duct are perturbed so that the normalized plane duct

cross-section Ω is [16]

$$\Omega = \left\{ (x,y) \in \mathbb{R}^2, -2 \leq x \leq 2, -1 + \epsilon_b g(x) \leq y \leq 1 + \epsilon_u f(x) \right\} \ (0 \leq \{\epsilon_b, \epsilon_u\} < 1). \tag{1}$$

The steady MHD flow equations are obtained from the momentum equations of fluid dynamics and from the steady Maxwell equations of electromagnetic through Ohm's law. Lorent'z force is included in the momentum equations. The steady MHD problem under consideration for the fluid normalized velocity V and the normalized induced magnetic field B is governed by the coupled non-dimensional equations [2, 26, 27]

$$\nabla^2 V + \mathrm{Ha}\frac{\partial B}{\partial y} = -1, \ \text{ and } \ \nabla^2 B + \mathrm{Ha}\frac{\partial V}{\partial y} = 0, \quad \text{in } \Omega, \tag{2}$$

where Ha is the Hartmann number given by $Ha = \dfrac{B_0 L \sqrt{\sigma}}{\sqrt{\mu}}$. B_0 and L are the applied magnetic field intensity and characteristic length, σ and μ electrical conductivity and fluid viscosity, respectively. $\nabla^2 = \dfrac{\partial^2}{\partial x^2} + \dfrac{\partial^2}{\partial y^2}$ is the two-dimensional Laplace operator.

Moreover, the adopted boundary conditions for the present work are [16–18, 26]

- For the insulated walls

$$V = B = 0 \text{ at } x = \pm 2, -1 \leq y \leq 1. \tag{3}$$

- For the perfectly conducting walls

$$V = 0, \quad \frac{\partial B}{\partial y} = 0 \text{ at } -2 \leq x \leq 2, y = -1 + \epsilon_b g(x), \text{ and } y = 1 + \epsilon_u f(x). \tag{4}$$

That is, the Hartmann walls are electrically perfectly conducting, side walls are insulated and the no-slip velocity is prescribed on each motionless walls. Moreover, the Hartmann number Ha occuring in (2) is defined as Ha $= L/d$ with $2L$ the duct undisturbed cross-section thickness in the y-direction and $d = (\mu/\sigma)B_0$ the Hartmann layer thickness. Recall that B_0 denotes the applied magnetic field intensity.

3 Stabilized FEM formulation

The MHD coupled Eq. (2) becomes convection dominated for large values of Ha for which the solution exhibits numerical oscillations. Thus, a stabilization procedure is required when the applied magnetic field is too strong. First, the standard Galerkin FEM (Finite Element Method) weak formulation of the Eq. (2) is given using the linear function spaces $L = (H_0^1(\Omega))^2$ and $L' = H^1(\Omega)$. This formulation consists in finding $\{V, B\} \in \{L \times L'\}$ such that:

$$a(\nabla V, \nabla v_1) - \ell\left(\mathrm{Ha}\frac{\partial B}{\partial y}, v_1\right) + a(\nabla B, \nabla v_2) - \ell(\mathrm{Ha}\frac{\partial V}{\partial y}, v_2) = \ell(1, v_1), \tag{5}$$

$\forall \{v_1, v_2\} \in \{L \times L'\}$ where $H^1(\Omega)$ is the Sobolev space of functions whose derivatives are square-integrable on Ω, $H_0^1(\Omega)$ is the subspace of $H^1(\Omega)$ of functions vanishing at $\partial\Omega$,

$$a(u,v) = \int_\Omega \left(\frac{\partial u}{\partial x}\frac{\partial v}{\partial x} + \frac{\partial u}{\partial y}\frac{\partial v}{\partial y} \right) d\Omega, \ \text{ and } \ \ell(u,v) = \int_\Omega (u\,v)\, d\Omega. \tag{6}$$

In order to apply the stabilized formulation to the Eq. (5) holding in the duct domain Ω, the Eq. (2) are decoupled first by defining the auxiliary normalized quantities $U_1 = V + B$ and $U_2 = V - B$. As a result, the Eq. (2) are recast into the following decoupled convection-diffusion type equations

$$\nabla^2 U_1 + \text{Ha}\frac{\partial U_1}{\partial y} = -1, \ \text{and} \ \nabla^2 U_2 - \text{Ha}\frac{\partial U_2}{\partial y} = -1 \ \ \text{in} \ \ \Omega. \tag{7}$$

The SUPG type stabilized formulation of the discretized Eq. (7) is written as in [25] in order to achieve a smooth behavior of the normalized velocity $V = (U_1 + U_2)/2$ and of the normalized induced magnetic field $B = (U_1 - U_2)/2$ due to the convection dominance at large values of Ha. That is, in a discretized scheme, find $\{U_{1_h}, U_{2_h}\} \in \{L_h' \times L_h'\}$ such that:

$$a(\nabla U_{1_h}, \nabla w_{1_h}) - \ell(\text{Ha}\frac{\partial U_{1_h}}{\partial y}, w_{1_h}) + a(\nabla U_{2_h}, \nabla w_{2_h}) + \ell(\text{Ha}\frac{\partial U_{2_h}}{\partial y}, w_{2_h})$$

$$+\tau_K \left\{ \ell(-\text{Ha}\frac{\partial U_{1_h}}{\partial y} - 1, -\text{Ha}\frac{\partial w_{1_h}}{\partial y}) + \ell(\text{Ha}\frac{\partial U_{2_h}}{\partial y} - 1, \text{Ha}\frac{\partial w_{2_h}}{\partial y}) \right\} \tag{8}$$

$$= \ell(1, w_{1_h}) + \ell(1, w_{2_h}).$$

$\forall \{w_{1_h}, w_{2_h}\} \in \{L_h' \times L_h'\}$ where L_h' is the space of linear functions defined on the discretized domain Ω_h obtained by discretizing Ω using triangles which are almost equally sized edges (i.e. almost uniform triangular dicretization). U_{1_h} and U_{2_h} are nodal values of U_1 and U_2 on Ω_h.

The stabilization parameter τ_K is taken as suggested in [25], i.e. as follows

$$\tau_K = \frac{h_K}{2\text{Ha}} \ \text{if} \ Pe_K \geq 1, \ \text{and} \ \tau_K = \frac{h_K^2}{12} \ \text{if} \ Pe_K < 1, \tag{9}$$

where h_K is the diameter of the element K ($h = max_K\{diam(K)\}$ as the mesh diameter), $Pe_K = h_K\frac{\text{Ha}}{6}$ is the Peclet number.

Finally, using the back transformations $V = (U_1 + U_2)/2$ and $B = (U_1 - U_2)/2$ one can get the final discretized system of stabilized Galerkin FEM equations for the velocity and the induced magnetic field as: find $\{V_h, B_h\} \in \{L_h \times L_h'\}$ such that :

$$a(\nabla V_h, \nabla v_{1_h}) - \ell(\text{Ha}\frac{\partial B_h}{\partial y}, v_{1_h}) + \tau_K \ell(\text{Ha}\frac{\partial V_h}{\partial y}, \text{Ha}\frac{\partial v_{1_h}}{\partial y})$$

$$+a(\nabla B_h, \nabla v_{2_h}) - \ell(\text{Ha}\frac{\partial V_h}{\partial y}, v_{2_h}) + \tau_K \ell(\text{Ha}\frac{\partial B_h}{\partial y}, \text{Ha}\frac{\partial v_{2_h}}{\partial y}) \tag{10}$$

$$= \ell(1, v_{1_h}) + \tau_K \ell(-1, \text{Ha}\frac{\partial v_{2_h}}{\partial y}),$$

where $\forall \{v_{1_h}, v_{2_h}\} \in \{L_h \times L'_h\}$.

After solving the system of Eq. (10) the velocity V of the fluid, and the induced current B in the duct, and on the perturbed upper and lower walls can be obtained. The obtained linear system of equations are saved in a sparse matrix form and the UMFPACK sparse system solver is used for the solution method. The algorithm of the developed code with GNU Fortran is given as follows;

Algorithm 1 Computer Code with GNU Fortran

Set : The problem parameters $Ha, \epsilon_u, \epsilon_b, f(x), g(x)$;

Define : The problem domain and mesh with linear triangular elements;

Set : $Ne = \#$ of elements; $Nn = \#$ of nodes;

for $i = 1$ to Ne **do**

    Calculate :

        The stabilization parameter τ_K

        Evaluate the integrals numerically using the Gaussian Quadrature method over triangle;

        Construct the element stiffness matrices and element load vectors;

        Assembly over the global system in the coupled form

    end for

Solve the obtained linear system with UMFPACK sparse solver;

---

4 Numerical results and discussion

Numerical solutions are obtained using FEM with SUPG stabilization. The velocity V and the induced magnetic field B are computed with 3-node triangular elements. The elements are obtained from almost a uniform cartesian grid. This grid is build by dividing the segment $[-1, 1]$ (for y) and $[-2, 2]$ (for x) into n_y and $n_x = 2n_y$ equal pieces, respectively (see Figure 2).

Before demonstrating the results of the proposed numerical scheme, the accuracy of the method is displayed in Table 1 by considering the Shercliff's problem where its exact solution can be found in [2]. Obtained numerical results are compared at for different points such that $P_1 = (-0.96, -0.96)$, $P_2 = (-0.76, -0.76)$, $P_3 = (-0.2, -0.4)$, $P_4 = (-0.5, 0)$. It is clearly seen that numerical results are in good agreement with exact ones even for the large values of Ha with at most 10^{-4} absolute error accuracy. The convergence, at given Hartmann number Ha, versus n_y has been carefully
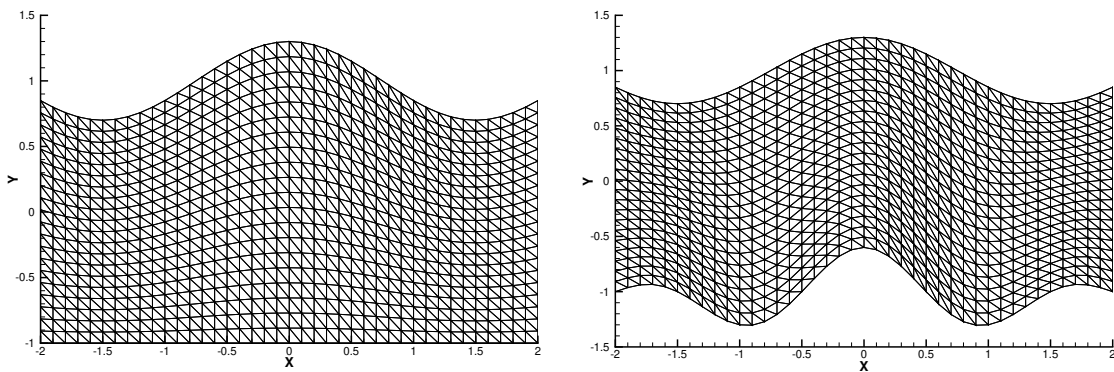

Figure 2. Sample meshes for $\epsilon_b = 0.0$, $f(x) = \cos(\frac{2\pi}{3}x)$, $\epsilon_u = 0.3$ (left) and $g(x) = (4 - x^2)\cos(\pi x)$, $\epsilon_b = 0.1$, $f(x) = \cos(\frac{2\pi}{3}x)$, $\epsilon_u = 0.3$ (right)

investigated for different values of ϵ_b, ϵ_u, and several shape functions $f(x)$. Such results are given

Table 1. Comparison of the obtained numerical results with the Shercliff's problem

Ha	Pt	$V_{numeric}$	V_{exact}	$B_{numeric}$	B_{exact}
5	P_1	0.0040551573	0.0040571532	0.0019567178	0.0019561903
	P_2	0.0614375686	0.0614409922	0.0304701196	0.0304717254
	P_3	0.1512387444	0.1512425023	0.0228402305	0.0228412750
	P_4	0.1557795360	0.1557876400	0.0629807968	0.0629877487
10	P_1	0.0042860284	0.0042870796	0.0027260465	0.0027247580
	P_2	0.0491422286	0.0491477810	0.0297616012	0.0297659763
	P_3	0.0906083175	0.0906100962	0.0160882297	0.0160890646
	P_4	0.0950492641	0.0950529002	0.0454468733	0.0454502087
50	P_1	0.0038485562	0.0038576025	0.0032355920	0.0032432695
	P_2	0.0166685274	0.0166697039	0.0119038202	0.0119048911
	P_3	0.0199796371	0.0199798098	0.0039837764	0.0039839310
	P_4	0.0199996447	0.0199996501	0.0099996447	0.0099996501
100	P_1	0.0028960461	0.0029085043	0.0025363846	0.0025480182
	P_2	0.0092913423	0.0092923891	0.0068920419	0.0068930820
	P_3	0.0099998726	0.0099998795	0.0019998786	0.0019998854
	P_4	0.0100000000	0.0100000000	0.0050000000	0.0050000000
500	P_1	0.0010937873	0.0011001732	0.0010137937	0.0010202377
	P_2	0.0019986959	0.0019987615	0.0015186959	0.0015187615
	P_3	0.0020000000	0.0020000000	0.0004000000	0.0004000000
	P_4	0.0020000000	0.0020000000	0.0010000000	0.0010000000

in Table 2 taking $\epsilon_b = 0$, $\epsilon_u = 0.3$ and $f(x) = \cos(\frac{2\pi}{3}x)$. This table gives the values of (V, B) at two points (Pt_1 and Pt_2) in the liquid and also minimum maximum values as B_{min}, B_{max} and V_{max}. As revealed by Table 2, it is sufficient to take $n_y = 80$ to ascertain a quite sufficient $\mathcal{O}(10^{-4})$ accuracy for each reported quantity. Accordingly, the computations presented in this paper are obtained for $n_y = 80$ (then $n_x = 160$).

Before testing the effects of the boundary perturbations on the flow, the effect of the stabilization on the solution is shown. It is seen from Figure 3 that, there are no significant differences in the magnetic induction solution curves whether the stabilization is used or not. In contrast, there are too many numerical instabilities in the velocity solution curves if the stabilization is not considered. It is well known from MHD duct flow characteristics that as Ha increases ($Ha > 10$) there is a stagnant region for the flow at the center of the duct. Without the stabilization, this behavior can not be caught as can be seen from Figure 3. The induced magnetic field develops only side and Hartmann layers as Ha increases. This is why it is not affected much by the SUPG stabilization. But for higher Ha values it will also need stabilization to get rid of the instabilities.

Then, the resulting FEM solution of the MHD duct flow is henceforth visualized in order to indicate how the flow adjusts to the presence of boundary perturbations.

First, we take $\epsilon_b = 0$ so that the lower plate is plane (i.e. with no perturbation), and $f(x) = \cos(\frac{2\pi}{3}x)$ for $x \in [-2, 2]$ which is a non-periodic boundary perturbation with upper wall symmetry with respect to $x = 0$. The velocity and the induced magnetic field profiles have been computed for $Ha \leq 500$ and for different values of the perturbation parameter ϵ_u.

Figure 4 presents the effects of the perturbation parameter $\epsilon_u = 0.1, 0.2, 0.3$ [16–18] on the flow velocity V and induced magnetic field B for $Ha = 5$. It is seen that, when $\epsilon_u = 0$ the flow forms two symmetric vortices with maximum magnitudes near the side walls (due to the length of the duct in x-direction and the direction of external magnetic field). An increase in ϵ_u forces the fluid to move through the perturbed boundary thereby weakening the side vortices and their magnitudes. The induced magnetic field B reaches its maximum value in the region near the

Table 2. The effect of the mesh size for the normalized velocity V and the induced magnetic field B values for $f(x) = \cos(\frac{2\pi}{3}x)$, $\epsilon_b = 0.0$ and $\epsilon_u = 0.3$

Ha	n_y	$Pt_1(0, 0.725)$		$Pt_2(1.5, 0.275)$		V_{max}	B_{min}	B_{max}
		V	B	V	B			
5	20	0.039878	-0.156582	0.048895	-0.056078	0.057069	-0.225322	0.143840
	40	0.040173	-0.156873	0.049056	-0.056261	0.057253	-0.225110	0.143683
	80	0.040247	-0.156948	0.049095	-0.056309	0.057303	-0.225057	0.143639
	160	0.040265	-0.156967	0.049105	-0.056321	0.057311	-0.225044	0.143628
10	20	0.010680	-0.082123	0.019204	-0.036305	0.025166	-0.127981	0.080573
	40	0.010746	-0.082214	0.019280	-0.036427	0.025242	-0.127960	0.080504
	80	0.010761	-0.082239	0.019297	-0.036459	0.025327	-0.127958	0.080488
	160	0.010764	-0.082245	0.019302	-0.036467	0.025331	-0.127958	0.080481
50	20	0.000408	-0.016375	0.000364	-0.007822	0.004332	-0.027464	0.018379
	40	0.000409	-0.016364	0.000349	-0.007826	0.004483	-0.027452	0.018457
	80	0.000409	-0.016364	0.000345	-0.007831	0.004564	-0.027452	0.018472
	160	0.000409	-0.016365	0.000344	-0.007833	0.004567	-0.027453	0.018478
100	20	0.000101	-0.008147	0.000045	-0.003679	0.002311	-0.013795	0.009424
	40	0.000101	-0.008134	0.000055	-0.003668	0.002223	-0.013782	0.009430
	80	0.000101	-0.008131	0.000054	-0.003664	0.002240	-0.013780	0.009442
	160	0.000101	-0.008131	0.000053	-0.003664	0.002258	-0.013780	0.009447
500	20	0.000004	-0.001619	0.000003	-0.000721	0.000336	-0.002765	0.002018
	40	0.000004	-0.001614	0.000004	-0.000715	0.000475	-0.002760	0.001971
	80	0.000004	-0.001612	0.000004	-0.000713	0.000441	-0.002758	0.001929
	160	0.000004	-0.001612	0.000004	-0.000713	0.000448	-0.002758	0.001931

maximum point of the curved boundary. This maximum value B_{max} of the induced magnetic field increases with an increase in ϵ_u.

In a similar manner, Figure 5, Figure 6 and Figure 7 show the effect of the perturbation parameter $\epsilon_u = 0.1, 0.3$ for Ha = 10, Ha = 50 and Ha = 500, respectively. As Ha increases, the flow is flattened (the velocity magnitude drops). Boundary layers are more pronounced near the side walls with thickness $\mathcal{O}(\frac{1}{\sqrt{Ha}})$ and near the Hartmann walls with thickness $\mathcal{O}(\frac{1}{Ha})$ as Ha increases as is mentioned as MHD flow characteristics in [26–28]. An increase in ϵ_u squeezes the vortices near the side walls developing a stagnant region at the center of the duct. Velocity and induced magnetic field profiles don't change anymore when both Ha and ϵ_u are further increased since they both cause strong boundary layers. Further increase in Ha (see Figure 6 for Ha = 50 and Figure 7 for Ha = 500) stops the effect of perturbed upper boundary on the velocity and induced magnetic field magnitudes and profiles. The flow is completely pushed to the side walls. The obtained results and trends are in good agreement with the results given in [16] in terms of level curves where they showed that perturbed boundary has a non-local impact on the flow and induced current.

Secondly, the effect of perturbed boundary on the velocity V and the induced magnetic field B is studied when the definition of the function $f(x)$ is changed for the upper wall. Figure 8, Figure 9 and Figure 10 show the flow and induced magnetic field behaviors for several upper wall functions in the same rectangular duct for Ha = 10. It is seen from these $V - B$ contours that, the effects of increasing the upper perturbation parameter for the functions $f(x) = \cos(\frac{\pi}{4}x)$, $f(x) = (4 - x^2)\cos(\pi x)$ and $f(x) = (4 - x^2)\sin(\pi x)$, respectively. The effect of the perturbed boundary is the same when different curves are used for the top wall shape. For small Ha, increasing ϵ_u decreases the velocity magnitude but increases the magnetic field values, especially

(a) Velocity without SUPG stabilization

(b) Magnetic induction without SUPG stabilization

(c) Velocity with SUPG stabilization

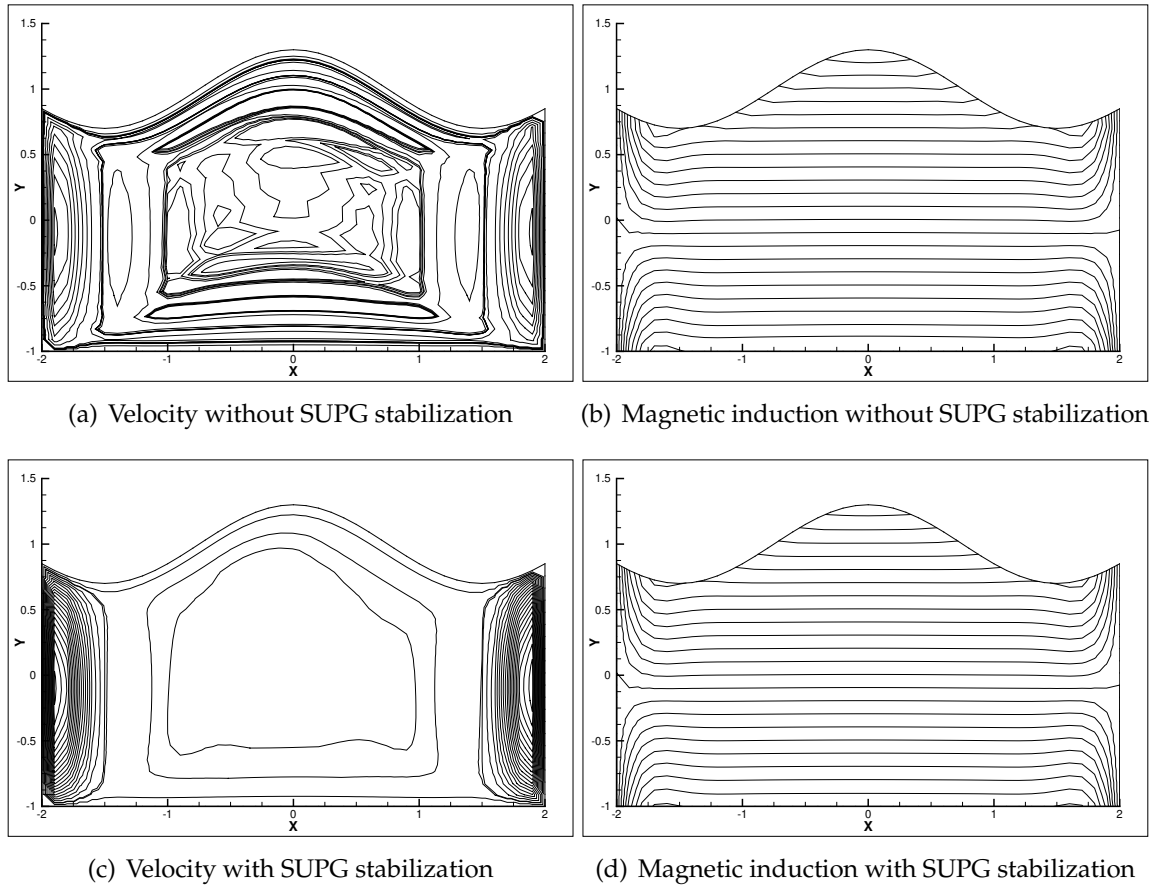(d) Magnetic induction with SUPG stabilization

Figure 3. The effect of stabilization on isolevel curves for the normalized velocity V and the induced magnetic field B for Ha $= 50$, $\epsilon_b = 0.0$, $f(x) = \cos(\frac{2\pi}{3}x)$ and $\epsilon_u = 0.3$

around the maximum region of the perturbed boundary. When Ha is further increased, such changes are not seen anymore since the well-known MHD characteristics dominate the flow and induced current as the formation of boundary layers.

Finally, the MHD flow and induced magnetic field have been computed for both bottom and upper disturbed boundaries taking Ha $= 5$ and Ha $= 50$. More precisely, three different cases are considered: identical perturbation functions ($g(x) = f(x) = (4 - x^2)\cos(\pi x)$) and perturbation parameters $\epsilon_b = \epsilon_u = 0.1$ in Figure 11, identical perturbation functions ($g(x) = f(x) = (4 - x^2)\cos(\pi x)$) but different perturbation parameters ($\epsilon_b = 0.1, \epsilon_u = 0.2$ in Figure 12 and $\epsilon_b = 0.2, \epsilon_u = 0.1$ in Figure 13), different perturbation functions ($g(x) = (4 - x^2)\sin(\pi x), f(x) = (4 - x^2)\cos(\pi x)$) with the same perturbation parameters ($\epsilon_b = \epsilon_u = 0.1$) in Figure 14. It is seen that, even if the bottom boundary is also perturbed, a stronger effect on the flow is still observed near the upper boundary due to the direction of the applied magnetic field (y-direction). The effect of the upper wall perturbations is the same as observed in Figure 8, Figure 9 and Figure 10 for changes of perturbation parameter or perturbation definition.

5 Conclusions

Steady MHD duct flow equations have been solved with the stabilized (FEM+SUPG) method for the curved Hartman walls seen as plane-perturbed boundaries. Variations in the perturbation parameters are found to strongly affect the flow and the induced magnetic field, especially near the perturbed upper boundary, and also show a noticeable impact far from the boundaries. If only the upper boundary is perturbed, the increase in the perturbation parameter forces the flow to
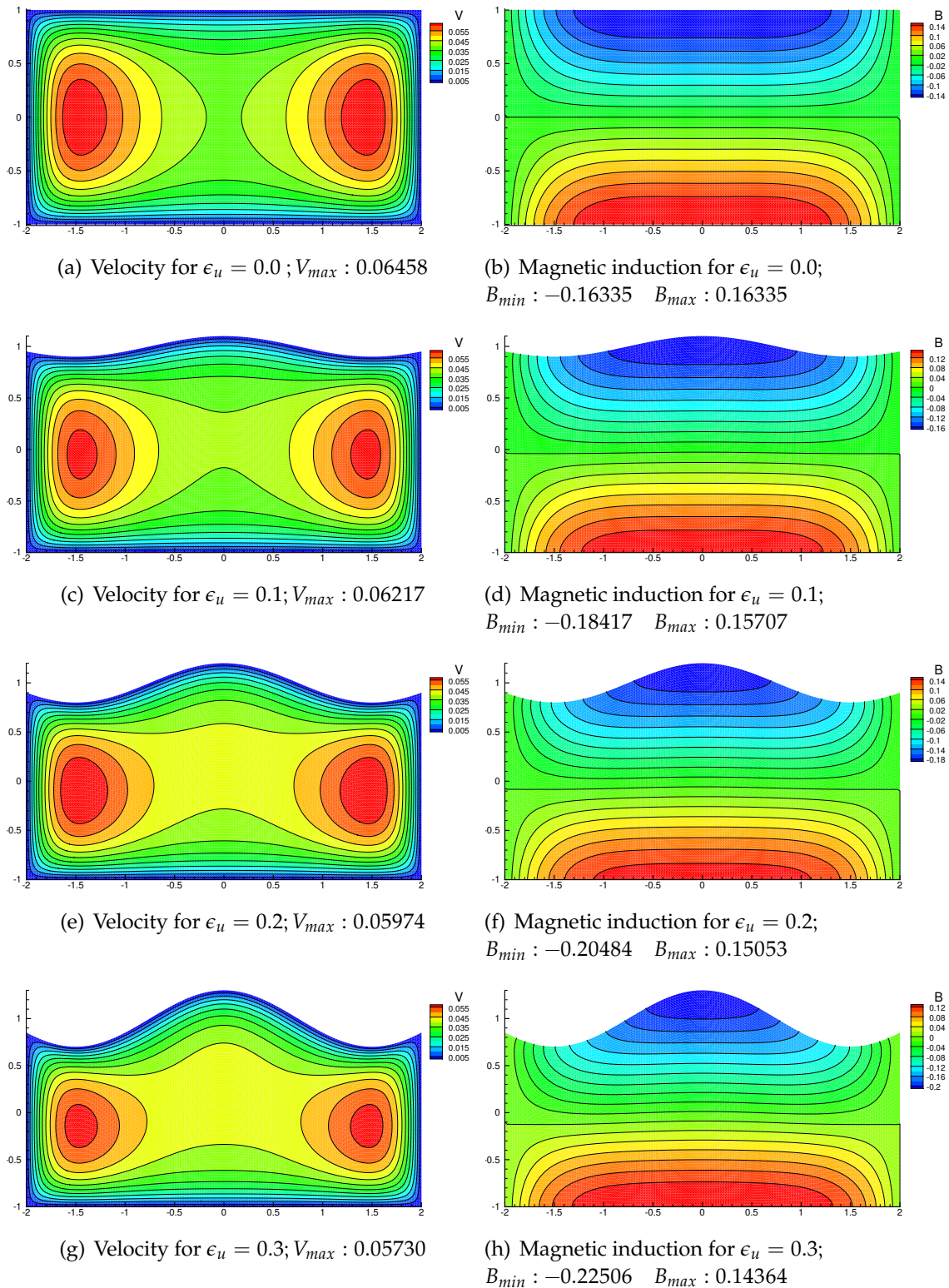
(a) Velocity for $\epsilon_u = 0.0$; $V_{max} : 0.06458$

(b) Magnetic induction for $\epsilon_u = 0.0$; $B_{min} : -0.16335$ $B_{max} : 0.16335$

(c) Velocity for $\epsilon_u = 0.1$; $V_{max} : 0.06217$

(d) Magnetic induction for $\epsilon_u = 0.1$; $B_{min} : -0.18417$ $B_{max} : 0.15707$

(e) Velocity for $\epsilon_u = 0.2$; $V_{max} : 0.05974$

(f) Magnetic induction for $\epsilon_u = 0.2$; $B_{min} : -0.20484$ $B_{max} : 0.15053$

(g) Velocity for $\epsilon_u = 0.3$; $V_{max} : 0.05730$

(h) Magnetic induction for $\epsilon_u = 0.3$; $B_{min} : -0.22506$ $B_{max} : 0.14364$

Figure 4. Isolevel curves for the normalized velocity V and induced magnetic field B for $Ha = 5$, $\epsilon_b = 0.0$, $f(x) = \cos(\frac{2\pi}{3}x)$ and $\epsilon_u = 0.1, 0.2, 0.3$.

move through this boundary, and the induced magnetic field increases reaching its maximum value in a region near the maximum point of the perturbed curve. Further, an increase in Ha delays the effect of the boundary perturbation leaving its place to a flattened flow with side layers and a stagnant flow at the central part of the duct. When both upper and bottom boundaries are perturbed, the stronger effect on the flow is seen again near the upper boundary compared to the
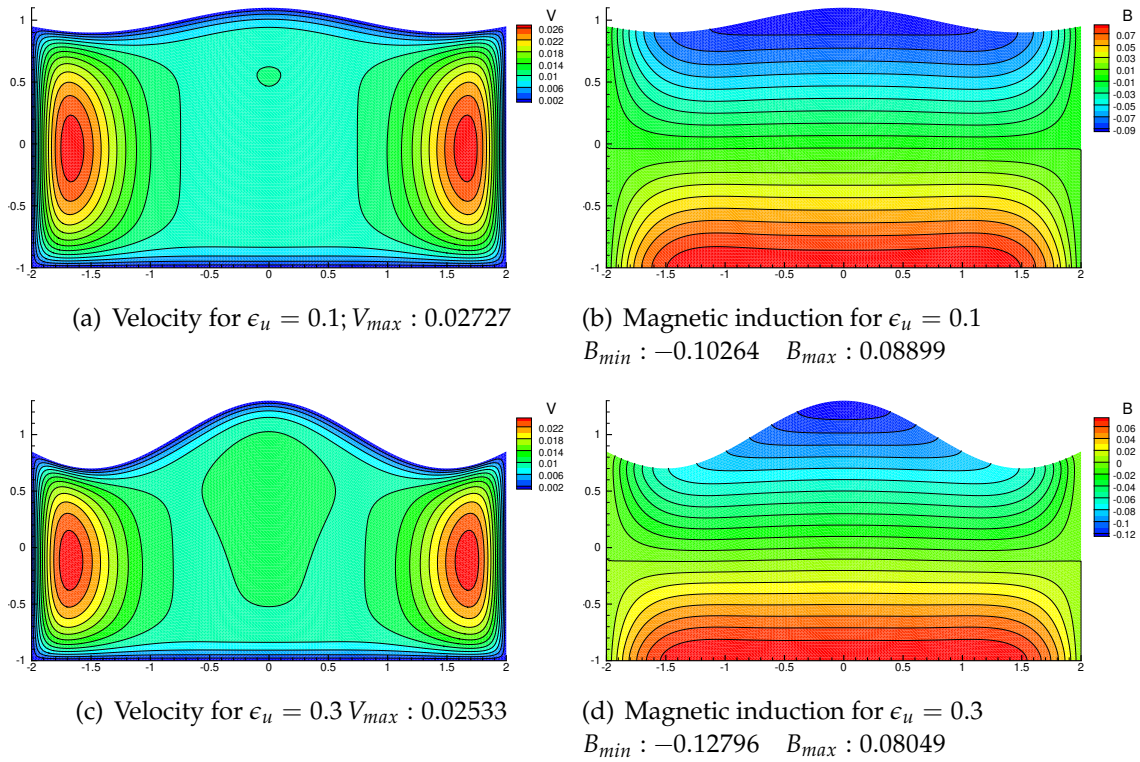
(a) Velocity for $\epsilon_u = 0.1$; V_{max} : 0.02727

(b) Magnetic induction for $\epsilon_u = 0.1$
B_{min} : -0.10264 B_{max} : 0.08899

(c) Velocity for $\epsilon_u = 0.3$ V_{max} : 0.02533

(d) Magnetic induction for $\epsilon_u = 0.3$
B_{min} : -0.12796 B_{max} : 0.08049

Figure 5. Isolevel curves for the normalized velocity V and induced magnetic field B for Ha $= 10$, $\epsilon_b = 0.0$, $f(x) = \cos(\frac{2\pi}{3}x)$ and $\epsilon_u = 0.1, 0.3$
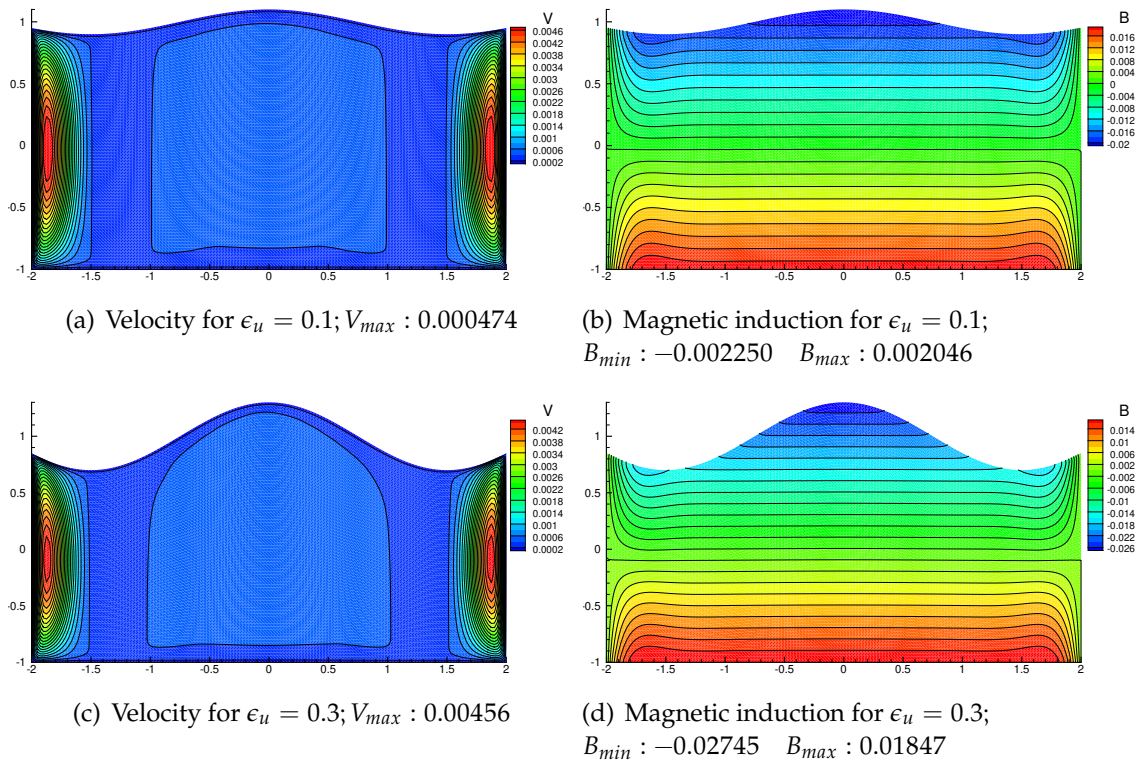

(a) Velocity for $\epsilon_u = 0.1$; V_{max} : 0.000474

(b) Magnetic induction for $\epsilon_u = 0.1$;
B_{min} : -0.002250 B_{max} : 0.002046

(c) Velocity for $\epsilon_u = 0.3$; V_{max} : 0.00456

(d) Magnetic induction for $\epsilon_u = 0.3$;
B_{min} : -0.02745 B_{max} : 0.01847

Figure 6. Isolevel curves for the normalized velocity V and induced magnetic field B for Ha $= 50$, $\epsilon_b = 0.0$, $f(x) = \cos(\frac{2\pi}{3}x)$ and $\epsilon_u = 0.1, 0.3$
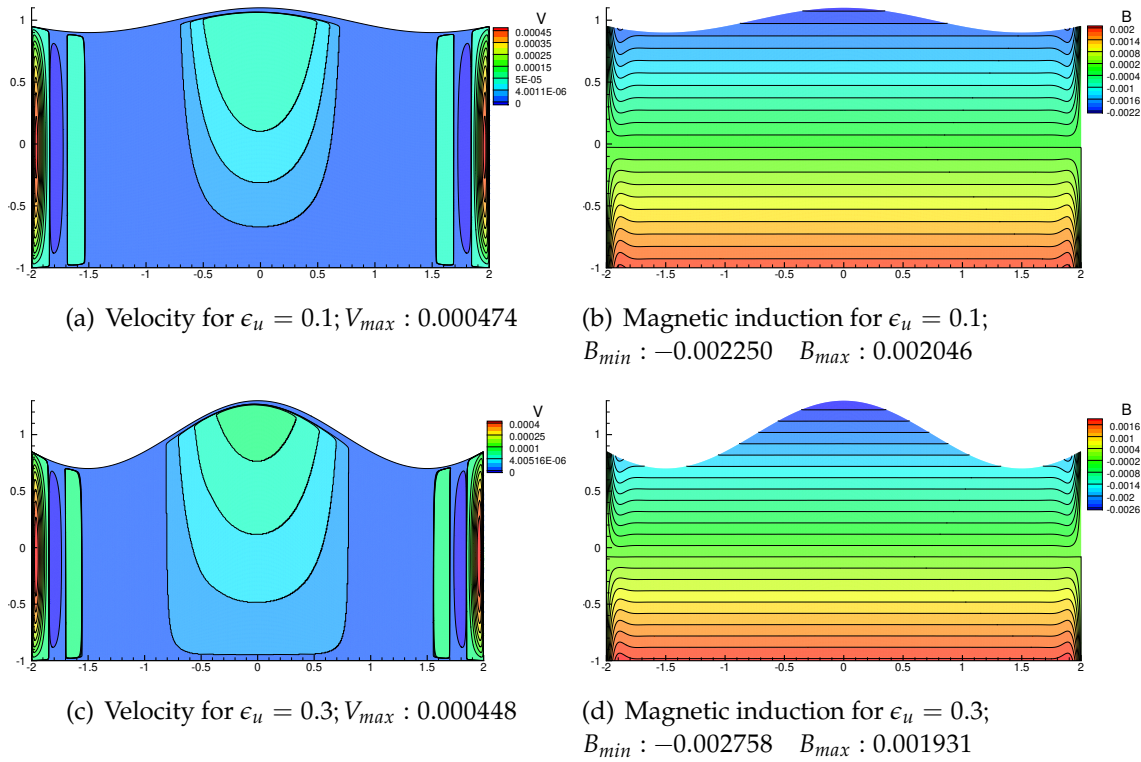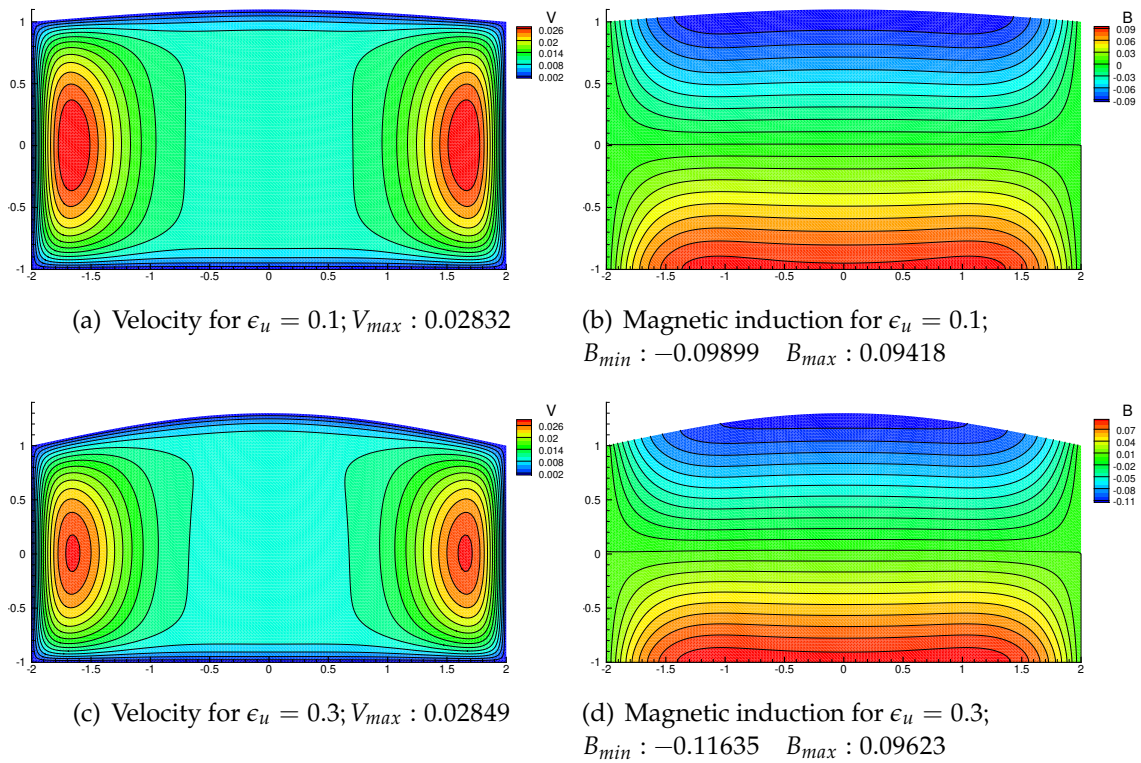
(a) Velocity for $\epsilon_u = 0.1$; $V_{max} : 0.000474$

(b) Magnetic induction for $\epsilon_u = 0.1$; $B_{min} : -0.002250$ $B_{max} : 0.002046$

(c) Velocity for $\epsilon_u = 0.3$; $V_{max} : 0.000448$

(d) Magnetic induction for $\epsilon_u = 0.3$; $B_{min} : -0.002758$ $B_{max} : 0.001931$

Figure 7. Isolevel curves for the normalized velocity V and induced magnetic field B for Ha $= 500$, $\epsilon_b = 0.0$, $f(x) = \cos(\frac{2\pi}{3}x)$ and $\epsilon_u = 0.1, 0.3$

(a) Velocity for $\epsilon_u = 0.1$; $V_{max} : 0.02832$

(b) Magnetic induction for $\epsilon_u = 0.1$; $B_{min} : -0.09899$ $B_{max} : 0.09418$

(c) Velocity for $\epsilon_u = 0.3$; $V_{max} : 0.02849$

(d) Magnetic induction for $\epsilon_u = 0.3$; $B_{min} : -0.11635$ $B_{max} : 0.09623$

Figure 8. Isolevel curves for the normalized velocity V and induced magnetic field B for Ha $= 10$, $\epsilon_b = 0.0$, $f(x) = \cos(\frac{\pi}{4}x)$

(a) Velocity for $\epsilon_u = 0.1$; V_{max} : 0.02891

(b) Magnetic induction for $\epsilon_u = 0.1$;
B_{min} : -0.12004 B_{max} : 0.09284

(c) Velocity for $\epsilon_u = 0.2$; V_{max} : 0.02959

(d) Magnetic induction for $\epsilon_u = 0.2$;
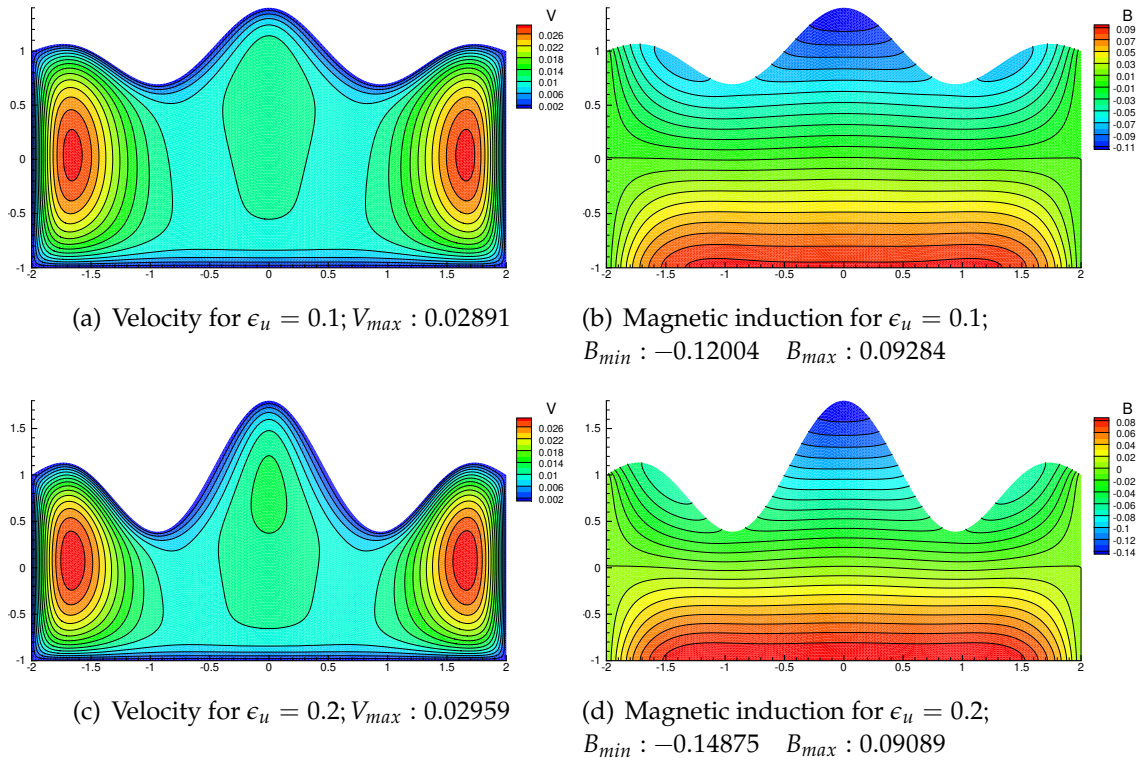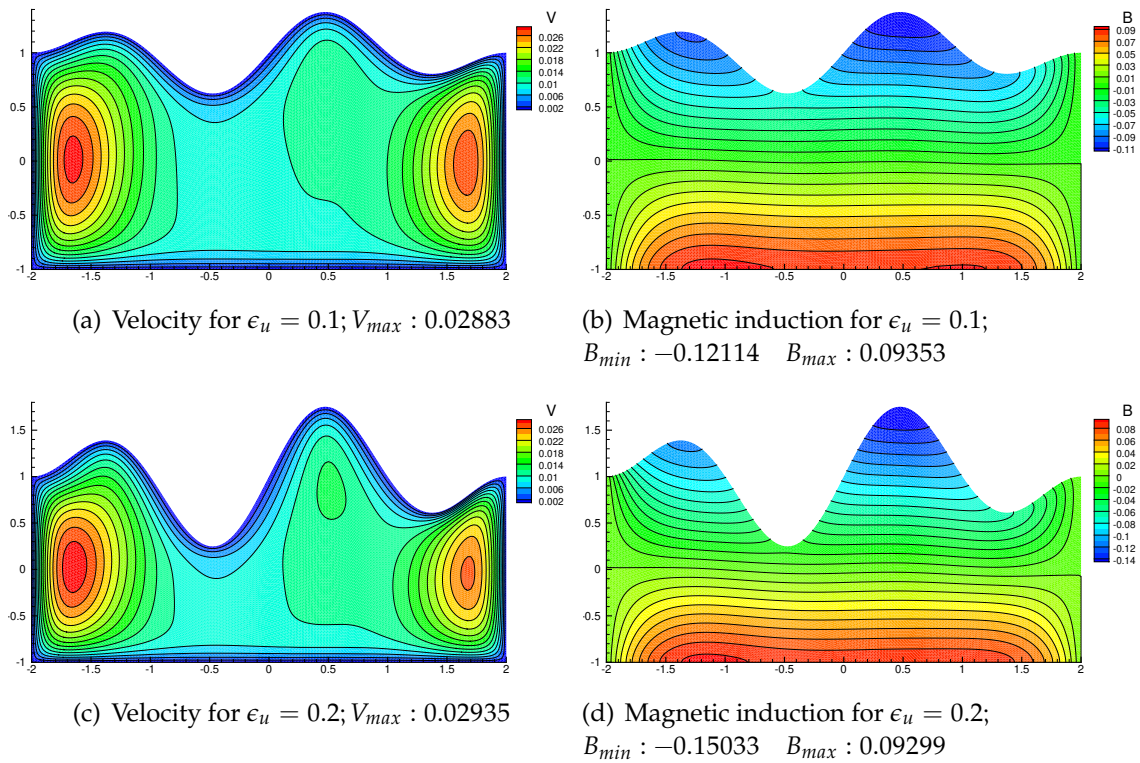B_{min} : -0.14875 B_{max} : 0.09089

Figure 9. Isolevel curves for the normalized velocity V and induced magnetic field B for Ha $= 10$, $\epsilon_b = 0.0$, $f(x) = (4 - x^2)\cos(\pi x)$ and $\epsilon_u = 0.1, 0.2$

(a) Velocity for $\epsilon_u = 0.1$; V_{max} : 0.02883

(b) Magnetic induction for $\epsilon_u = 0.1$;
B_{min} : -0.12114 B_{max} : 0.09353

(c) Velocity for $\epsilon_u = 0.2$; V_{max} : 0.02935

(d) Magnetic induction for $\epsilon_u = 0.2$;
B_{min} : -0.15033 B_{max} : 0.09299

Figure 10. Isolevel curves for the normalized velocity V and induced magnetic field B for Ha $= 10$, $\epsilon_b = 0.0$, $f(x) = (4 - x^2)\sin(\pi x)$ and $\epsilon_u = 0.1, 0.2$

(a) Velocity for Ha = 5; V_{max} : 0.06420

(b) Magnetic induction for Ha = 5;
B_{min} : -0.19989 B_{max} : 0.18578

(c) Velocity for Ha = 50; V_{max} : 0.00498

(d) Magnetic induction for Ha = 50;
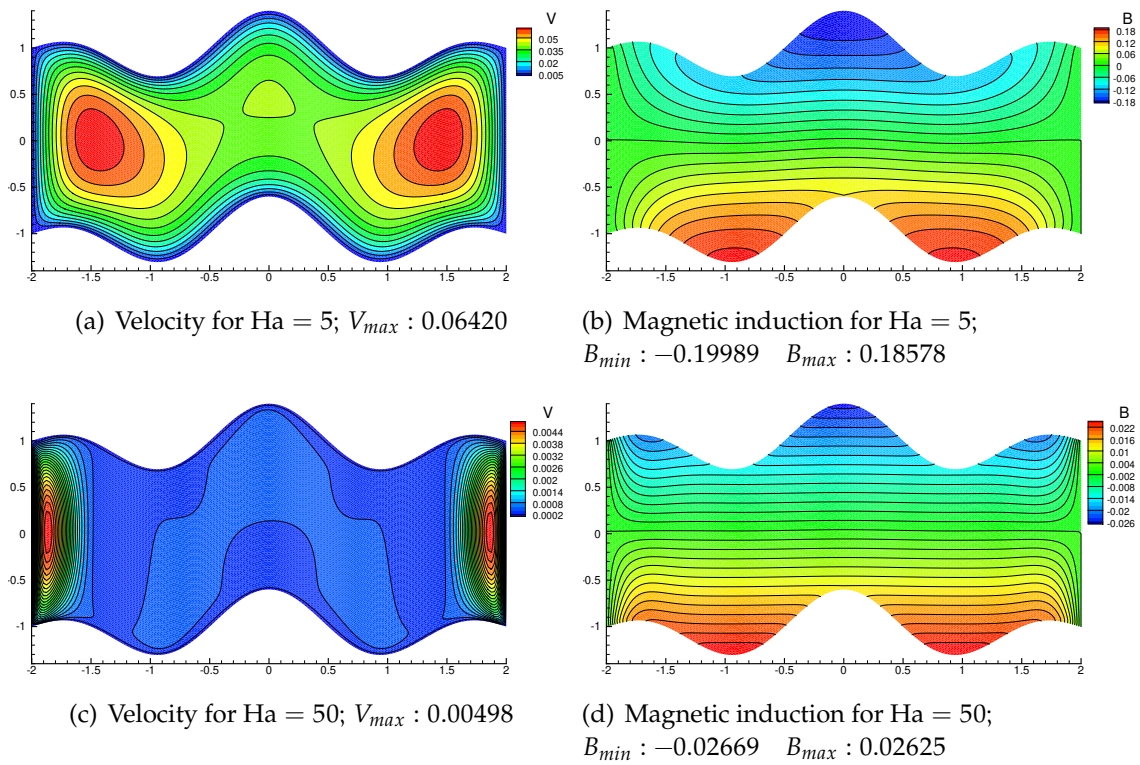B_{min} : -0.02669 B_{max} : 0.02625

Figure 11. Isolevel curves for the normalized velocity V and induced magnetic field B for $\epsilon_b = 0.1$, $g(x) = (4 - x^2)\cos(\pi x)$, $\epsilon_u = 0.1$, $f(x) = (4 - x^2)\cos(\pi x)$ and Ha = 5, 50
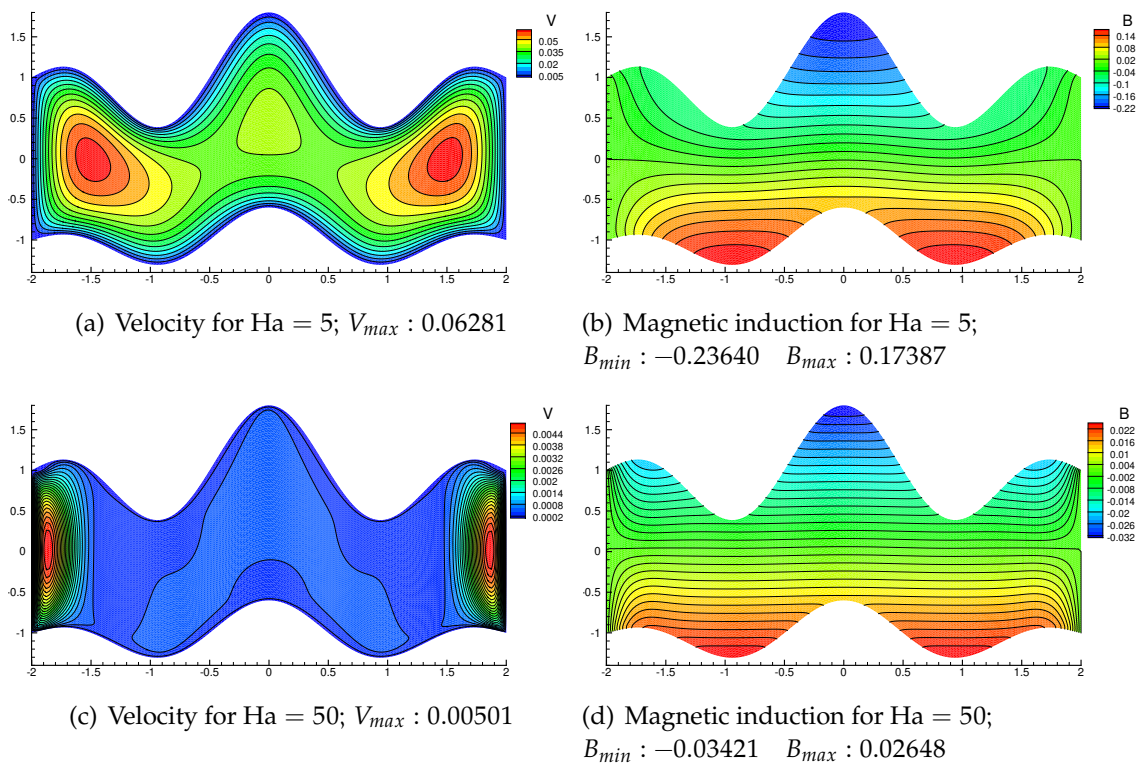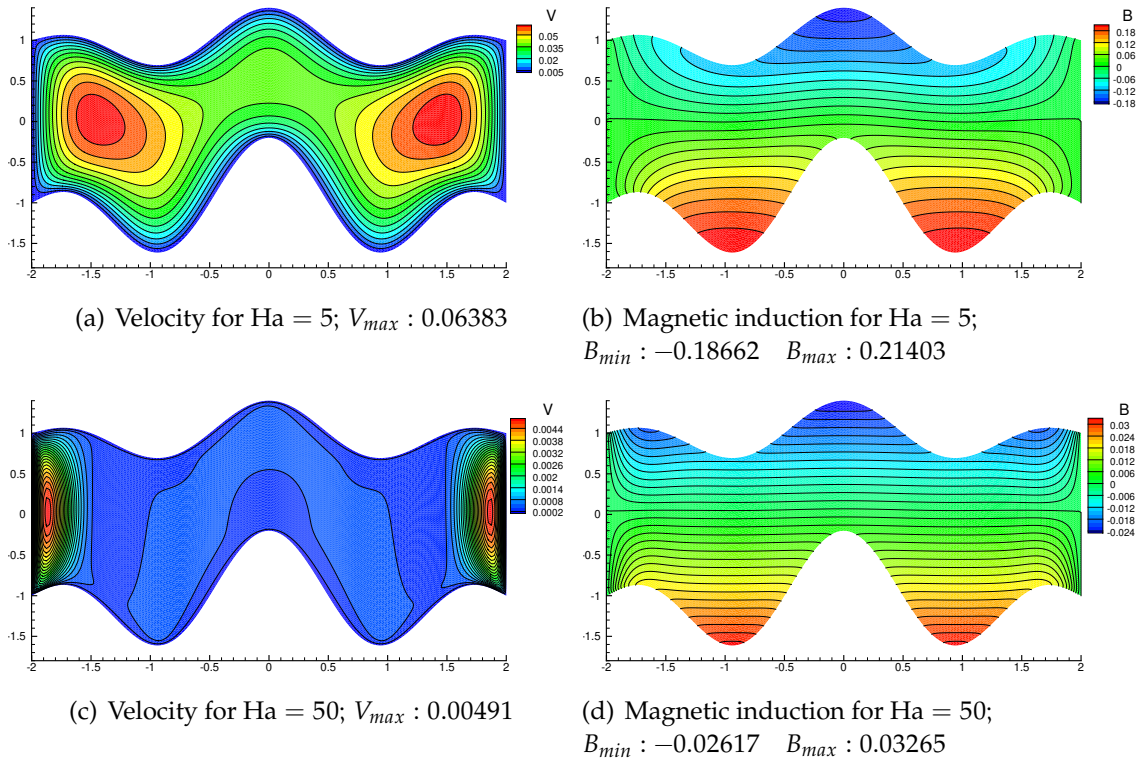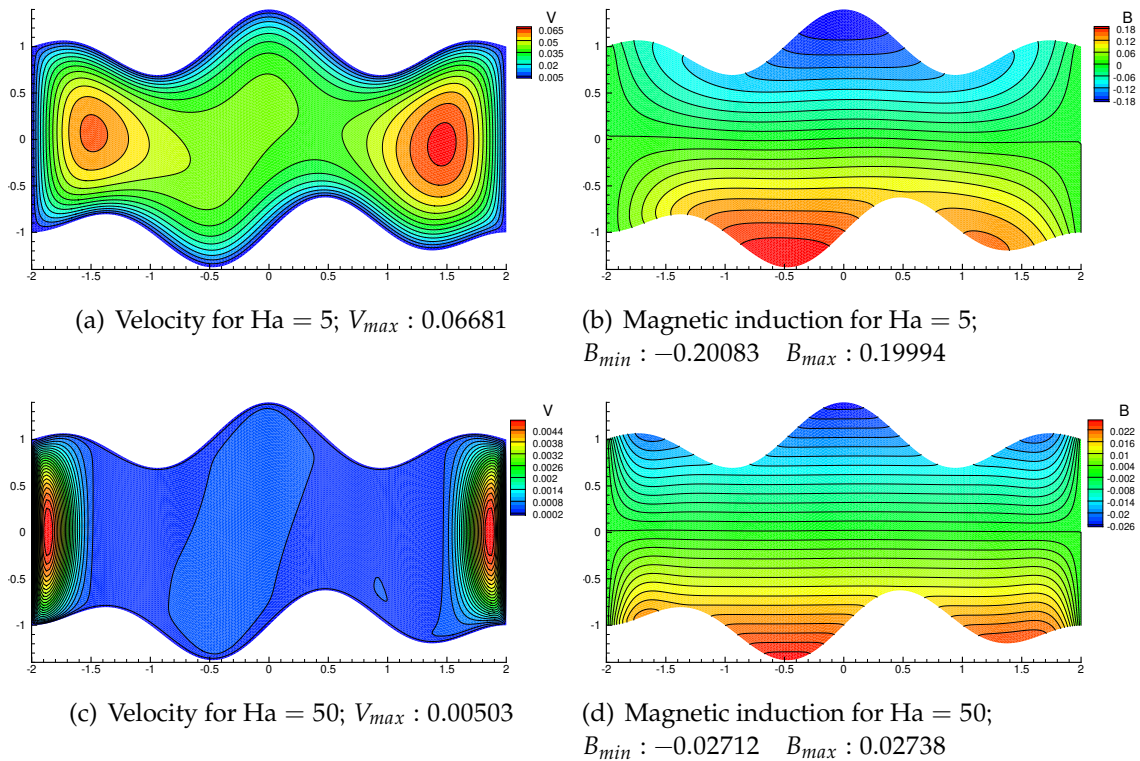

(a) Velocity for Ha = 5; V_{max} : 0.06281

(b) Magnetic induction for Ha = 5;
B_{min} : -0.23640 B_{max} : 0.17387

(c) Velocity for Ha = 50; V_{max} : 0.00501

(d) Magnetic induction for Ha = 50;
B_{min} : -0.03421 B_{max} : 0.02648

Figure 12. Isolevel curves for the normalized velocity V and induced magnetic field B for $\epsilon_b = 0.1$, $g(x) = (4 - x^2)\cos(\pi x)$, $\epsilon_u = 0.2$, $f(x) = (4 - x^2)\cos(\pi x)$ and Ha = 5, 50

(a) Velocity for Ha = 5; V_{max} : 0.06383

(b) Magnetic induction for Ha = 5; $B_{min} : -0.18662 \quad B_{max} : 0.21403$

(c) Velocity for Ha = 50; V_{max} : 0.00491

(d) Magnetic induction for Ha = 50; $B_{min} : -0.02617 \quad B_{max} : 0.03265$

Figure 13. Isolevel curves for the normalized velocity V and induced magnetic field B for $\epsilon_b = 0.2$, $g(x) = (4 - x^2)\cos(\pi x)$, $\epsilon_u = 0.1$, $f(x) = (4 - x^2)\cos(\pi x)$ and Ha = 5, 50

(a) Velocity for Ha = 5; V_{max} : 0.06681

(b) Magnetic induction for Ha = 5; $B_{min} : -0.20083 \quad B_{max} : 0.19994$

(c) Velocity for Ha = 50; V_{max} : 0.00503

(d) Magnetic induction for Ha = 50; $B_{min} : -0.02712 \quad B_{max} : 0.02738$

Figure 14. Isolevel curves for the normalized velocity V and induced magnetic field B for $\epsilon_b = 0.1$, $g(x) = (4 - x^2)\sin(\pi x)$, $\epsilon_u = 0.1$, $f(x) = (4 - x^2)\cos(\pi x)$ and Ha = 5, 50

bottom one, because of the direction of the applied magnetic field. The proposed and implemented stabilized FEM procedure well captures all the influences of the perturbed boundaries on the MHD rectangular duct flow even at large Hartmann numbers, i.e. in the case of convection dominance (case of a strong external magnetic field). The findings of the computed results, for the velocity profile and induced magnetic field changes due to the boundary perturbations of the duct, can be made use of in the liquid metal blanket design and blood flow measurements in the constricted vessels. This solution procedure can also be extended to completely arbitrary-shaped ducts.

Nomenclature

μ	Viscosity
σ	Electrical conductivity
Ω	Domain
$\partial\Omega$	Domain boundary
Ω_h	Discretized domain
B_0	Applied magnetic field intensity
$H_0^1(\Omega)$	Sobolov space
L	Characteristic length and $L = H_0^1(\Omega)$ Square integrable functions
$L' = H^1(\Omega)$	Derivatives are square integrable functions
L_h and L_h'	Functions defined on the discretized domain
Ha	Hartmann number
B	Magnetic field
V	Velocity $(U_1 = V + B, U_2 = V - B)$
p	Pressure
ϵ_u	Upper boundary perturbation parameter
ϵ_b	Lower boundary perturbation parameter
$f(x)$	Upper boundary shape function
$g(x)$	Lower boundary shape function
τ_K	Stabilization parameter
Pe_K	Peclet number
h_K	Diameter of the element K
n_y	Number of pieces on side walls
$n_x = 2n_y$	Number of pieces on upper and lower walls
Pt_1, Pt_2	Point 1, Point 2

Declarations

Use of AI tools

The authors declare that they have not used Artificial Intelligence (AI) tools in the creation of this article.

Data availability statement

No Data associated with the manuscript.

Ethical approval (optional)

The authors state that this research complies with ethical standards. This research does not involve either human participants or animals.

Consent for publication

Not applicable

References

[1] Hartmann, J. Theory of the laminar flow of an electrically conductive liquid in a homogeneous magnetic field. *K. Dan. Vidensk. Selsk. Mat. Fys. Medd.,* 15(6), 1-28, (1937).

[2] Shercliff, J.A. Steady motion of conducting fluids in pipes under transverse magnetic fields. In Proceedings, *Mathematical Proceedings of the Cambridge Philosophical Society* pp. 136-144. Cambridge University Press, (1953, January). [CrossRef]

[3] Singh, B. and Lal, J. MHD axial flow in a triangular pipe under transverse magnetic field. *Indian Journal of Pure and Applied Mathematics,* 18, 101-115, (1978).

[4] Singh B. and Jia L. MHD axial flow in a triangular pipe under transverse magnetic field parallel to a side of the triangle. *Indian Journal of Pure and Applied Mathematics,* 9(2), 101-115, (1978).

[5] Sheu, T.W.H. and Lin, R.K. Development of a convection–diffusion-reaction magnetohydrodynamic solver on non-staggered grids. *International Journal for Numerical Methods in Fluids,* 45(11), 1209-1233, (2004). [CrossRef]

[6] Singh, B. and Lal, J. FEM in MHD channel flow problems. *International Journal for Numerical Methods in Engineering,* 18, 1104-1111, (1982).

[7] Singh, B. and Lal, J. Finite element method for unsteady MHD flow through pipes with arbitrary wall conductivity. *International Journal for Numerical Methods in Fluids,* 4(3), 291-302, (1984). [CrossRef]

[8] Tezer-Sezgin, M. and Koksal, S. Finite element method for solving MHD flow in a rectangular duct. *International Journal for Numerical Methods in Engineering,* 28(2), 445-459, (1989). [CrossRef]

[9] Tezer-Sezgin, M. Boundary element method solution of MHD flow in a rectangular duct. *International Journal for Numerical Methods in Fluids,* 18(10), 937-952, (1994). [CrossRef]

[10] Tezer-Sezgin, M. and Bozkaya, C. Boundary element method solution of magnetohydrodynamic flow in a rectangular duct with conducting walls parallel to applied magnetic field. *Computational Mechanics,* 41, 769-775, (2008). [CrossRef]

[11] Tezer-Sezgin, M. and Han Aydın, S. Dual reciprocity boundary element method for magnetohydrodynamic flow using radial basis functions. *International Journal of Computational Fluid Dynamics,* 16(1), 49-63, (2002). [CrossRef]

[12] Tezer-Sezgin, M. Solution of magnetohydrodynamic flow in a rectangular duct by differential quadrature method. *Computers & Fluids,* 33(4), 533-547, (2004). [CrossRef]

[13] Tezer-Sezgin, M. and Bozkaya, C. *Boundary Element Method for Magnetohydrodynamic Flow: 2D MHD Duct Flow Problems*, (Vol. 14). Springer Nature: Switzerland, (2024). [CrossRef]

[14] Neslituurk, A.I. and Tezer-Sezgin, M. The finite element method for MHD flow at high Hartmann numbers. *Computer Methods in Applied Mechanics and Engineering,* 194(9-11), 1201-1224, (2005). [CrossRef]

[15] Neslituurk, A.I. and Tezer-Sezgin, M. Finite element method solution of electrically driven magnetohydrodynamic flow. *Journal of Computational and Applied Mathematics,* 192(2), 339-352, (2006). [CrossRef]

[16] Mahabaleshwar, U.S. Pazanin, I. Radulovic, M. and Suárez Grau. F.J. Effects of small boundary perturbation on the MHD duct flow. *Theoretical and Applied Mechanics,* 44(1), 83-101, (2017). [CrossRef]

[17] Aydin, C. and Tezer-Sezgin, M. DRBEM solution of the Cauchy MHD duct flow with a slipping perturbed boundary. *Engineering Analysis with Boundary Elements,* 93, 94-104, (2018). [CrossRef]

[18] Fendoğlu, H., Bozkaya, C. and Tezer-Sezgin, M. MHD flow in a rectangular duct with a perturbed boundary. *Computers & Mathematics with Applications,* 77(2), 374-388, (2019). [CrossRef]

[19] Yang, L., Mao, J. and Xiong, B. Numerical simulation of liquid metal MHD flows in a conducting rectangular duct with triangular strips. *Fusion Engineering and Design,* 163, 112152, (2021). [CrossRef]

[20] Okechi, N.F., Asghari S. and Charreh, D. Magnetohydrodynamic flow through a wavy curved channel. *AIP Advances,* 10(3), 035114, (2020). [CrossRef]

[21] Marušić–Paloka, E., Pazanin, I. and Radulovic, M. MHD flow through a perturbed channel filled with a porous medium. *Bulletin of the Malaysian Mathematical Sciences Society*, 45, 2441-2471, (2022). [CrossRef]

[22] Prasanna Jeyanthi, M. and Ganesh, S. Numerical solution of magnetohydrodynamic flow through duct with perturbated boundary using RBF-FD method. *International Journal of Ambient Energy*, 45(1), 2276130, (2024). [CrossRef]

[23] Tezer-Sezgin, M. and Han Aydin, S. The Stabilized FEM Solution of the MHD Flow in a Rectangular Duct with Perturbed Boundary. *CMES 2018 (presentation), 3rd International Conference on Computational Mathematics and Engineering Sciences,* 04-06 May 2018, Girne, Cyprus.

[24] Tezer-Sezgin, M. and Han Aydın, S. Steady MHD Flow in a Duct with Non-Rectangular Cross-Section Using the Stabilized FEM Solution. *ICAME 24, The 3rd International Conference on Applied Mathematics in Engineering,* 26-28 June 2024, Balikesir, Türkiye.

[25] Brooks, A.N. and Hughes. T.J.R. Streamline upwind/Petrov-Galerkin formulations for convection dominated flows with particular emphasis on the incompressible Navier-Stokes equations. *Computer Methods in Applied Mechanics and Engineering,* 32(1-3), 199-259, (1982). [CrossRef]

[26] Müller, U. and Bühler, L. *Magnetofluiddynamics in Channels and Containers*. Springer-Verlag: Berlin, (2001).

[27] Moreau, R.J. *Magnetohydrodynamics, Fluid Mechanics and its applications*, Kluwer Academic

Publisher, (1990).

[28] Branover, G.G and Tsinober, A. B. *Magnetohydrodynamic of incompressible media*, Moscow: Nauka, (1970).

Mathematical Modelling and Numerical Simulation with Applications (MMNSA)
(https://dergipark.org.tr/en/pub/mmnsa)